Silica based binary glass systems - refractive index behaviour and composition in optical fibres

C. R. HAMMOND, S. R. NORMAN
Department of Electronics, University of Southampton, Southampton SO9 5NH.

Refractive index versus composition data are presented for three silica based binary glass systems SiO_2–B_2O_3, SiO_2–P_2O_5 and SiO_2–GeO_2. Using a near-field scanning method refractive index measurements were made on graded-index optical fibres, of known composition, fabricated by the chemical vapour deposition technique. The experimental data for each glass system is also compared with theoretical predictions of refractive index versus composition made from a single oscillator, Sellmeier model involving an oscillator energy and a dispersion energy term.

1. Introduction
1.1. Optical fibres
In order to fabricate fibre optic waveguides from low-loss synthetic silica a second glass is required which has a different refractive index, but which is also sufficiently mechanically compatible with silica in terms of viscosity and expansion coefficient, to be fabricated into a fibre. The approach generally adopted is to modify the properties of silica by the addition of other glass forming components (usually oxides), producing a silica based binary glass which has a lower or greater refractive index than silica. This has resulted in the development of a number of techniques and materials, amongst them variations of the chemical vapour deposition (CVD) technique to produce phosphosilicate glass [1], germania–silica glass [2, 3] and borosilicate glass [3–5] in fibres.

To operate fibre communications systems at high data rates fibres with low dispersion are required. One means of achieving this is by careful grading of the refractive index profile in the fibre core. By fabricating a nearly-parabolic profile, equalization of the mode transit times is obtained, and waveguide (modal) dispersion is considerably reduced [6]. The ideal profile parameter $\alpha_{opt}(\sim 2)$ depends on the wavelength of operation and on the variation of the refractive index with wavelength [7–11]. In order to fabricate accurately a given profile it is necessary to know how the refractive index of the binary silica glass within the fibre varies with composition.

1.2. Bulk glasses and glasses in fibres
A number of papers give details of refractive index as a function of composition for the binary glasses SiO_2–B_2O_3 [9, 12, 13], SiO_2–GeO_2 [9, 13] and SiO_2–P_2O_5 [13]. However, these are nearly all measurements made on bulk annealed samples of binary glasses prepared by crucible melting of powdered oxides. It is well known that the physical and mechanical properties of glass in the fibre form differ greatly from those of the bulk form of the same glass [14, 15].

In the case of the fibre, where the fibre drawing process imposes severe quenching or chilling of the glass, any attempt at an explanation of measured properties must be based on the thermal history of the glass in the fibre. In our drawing process for these silica based fibres the thermal history includes a quenching from 2100° C to room temperature in less than a second. Generally it can be stated that the physical properties of the fibre formed in the drawing process correspond with the properties of the glass at some elevated temperature (the fictive temperature). Thus the glass in the fibre should differ from the annealed bulk form of the glass by having a lower density and refractive index [14].

Consequently, data relating refractive indices

and refractive index dispersion to glass composition for bulk annealed glass samples cannot really be extended to an analysis of a fibre, fabricated from the same glass system, in terms of pulse dispersion and ideal profile parameter [9]. The most desirable approach is to use refractive index data, for the given glass system, obtained from fibres and hence subjected to the quenching inherent in the drawing process.

1.3. Achievements of this work

This paper reports the measurement of refractive indices against composition, in optical fibres, for the three most commonly used silica-based binary glass systems: SiO_2–B_2O_3, SiO_2–P_2O_5 and SiO_2–GeO_2. In addition the results can be interpreted in terms of a Sellmeier dispersion model, which is based on the properties of the end member components of the binary system, and follows the method used by Wemple *et al.* [12] to explain data from annealed bulk samples of SiO_2–B_2O_3 glass.

2. Experimental procedure
2.1. Chemical vapour deposition of the fibre preforms

Using the chemical vapour deposition technique developed by Gambling *et al.* [16] a number of glass fibre optical waveguides were fabricated with core glasses from the three silica-based binary systems listed above.

Two fibres were fabricated with cores of phosphosilicate glass (fibres numbered VD/102 and VD/138). During the core deposition the P_2O_5 concentration in the glass was linearly increased with each layer from zero to a maximum of 16.5 mol % and 18 mol % for VD/138 and VD/102 respectively. After the subsequent collapse to a preform and drawing into a fibre, this should result in a near parabolic distribution of P_2O_5 (and hence refractive index increase) radially across the fibre core.

Similarly two fibres were fabricated with cores of germania–silica glass, with the GeO_2 concentrations increased linearly to 5 mol % and 11 mol % (fibres VD/160 and VD/161 respectively). These fibres also had a small constant amount of P_2O_5 (3 mol %) included in the core to help fusion of the core layers. This was allowed for in the refractive index difference calculations

$(\Delta n(3 \text{ mol } \% \text{ } P_2O_5) \simeq 2 \times 10^{-3})$. Finally a single fibre was fabricated from borosilicate glass (VD/143). As the borosilicate glass system gives refractive indices less than that of pure silica a slightly different technique was adopted. In the first four layers the B_2O_3 concentration was rapidly increased in steps of 5 mol % to 20 mol %, and then 15 layers were deposited with a constant 20 mol % B_2O_3 to form a cladding. Finally the B_2O_3 concentration was linearly reduced from 20 mol % to zero with each core layer deposited and finishing with a layer of pure silica.

2.2. Correction of doping levels in the fibres

The dopant (P_2O_5, GeO_2 or B_2O_3) level in the silica of each deposited layer is set by controlling carrier gas flows, containing vapours of appropriate volatile halides ($POCl_3$, $GeCl_4$, BBr_3 and $SiCl_4$), during the CVD process [16]. There are thus the possibilities that (a) a carrier gas stream after bubbling through its particular liquid halide may carry a smaller amount of vapour than expected due to incomplete vapour saturation, and (b) that the deposited glass composition may not follow that set by the carrier gas streams.

The first problem can easily be overcome with the use of suitable mass–flow controllers for each halide, however as we are limited to bubbling our carrier gases through Dreschel bottles, the vaporization efficiencies of each halide bubbler were measured and corrections applied to find true concentration levels. Consequently during the fibre preform deposition each halide bubbler was weighed before and after to give the actual mass of halide vaporized. Knowing the flow rate and duration of carrier gas flow the theoretical mass loss can be calculated from the halide vapour pressure. The ratio of actual mass loss to theoretical mass loss defined an average vaporization efficiency for that halide bubbler for that deposition. Typically for $POCl_3$ the vaporization efficiency lies between 0.5 and 0.7, depending on halide temperature, carrier gas temperature, liquid height and to a lesser extent carrier flow rate, while the corresponding figure for $SiCl_4$ is more or less constant at 0.9. For a particular dopant–silica combination, it is the ratio of dopant vaporization efficiency to silica vaporization efficiency that is used to give true doping levels.
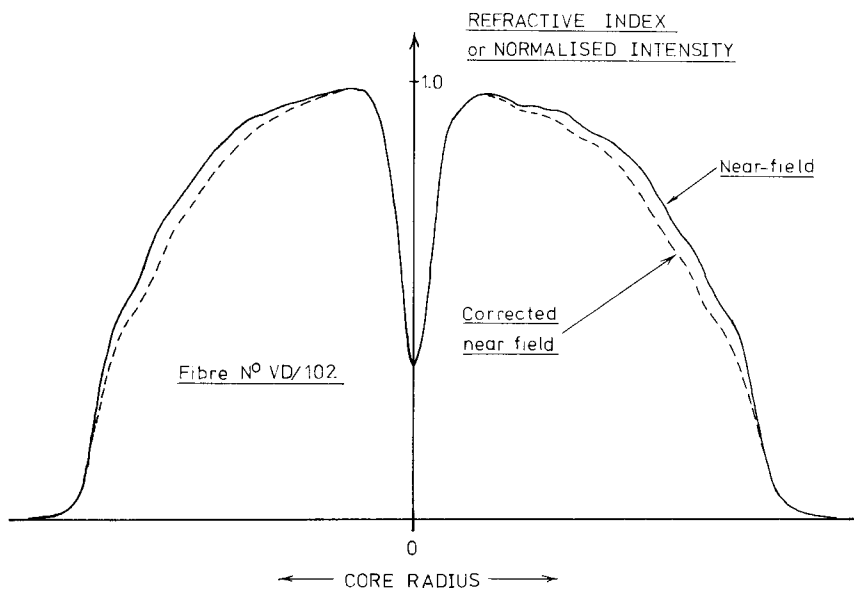
Microprobe and etch-rate analysis has shown

Figure 1 Solid curve: near-field intensity distribution for fibre VD/102. Dashed curve: normalized index-profile after leaky-mode correction of fibre VD/102.

that for $SiO_2-P_2O_5$ core fibres the deposited glass composition does closely follow that of the carrier gas streams, for concentrations below about 15 mol % and provided high deposition temperatures are not used. Also French *et al.* [21] have shown by X-ray analysis that the composition of $SiO_2-B_2O_3$ glass in fibres closely follows that set by the reactant vapour stream (BCl_3 and $SiCl_4$ in O_2). Finally microprobe analysis of some of our SiO_2-GeO_2 fibres has shown that the GeO_2 concentrations are only ~ 30% of that set by the vapour reactants during CVD. Consequently microprobe Ge-concentration profiles have been used to determine the true doping levels for each layer in these fibre cores.

2.3. Fibre drawing

The fibre preforms were drawn on a precision fibre drawing machine [16] using a graphite resistance furnace [16, 17] into fibres of between 0.8 and 1 km length. The number of core layers and pulling conditions were adjusted to give fibres of outside diameter $150 \mu m$ and $50 \mu m$ core diameter.

3. Fibre evaluation

3.1. Near field scanning measurements

The near-field scanning technique developed by Sladen *et al.* [18] provides a simple and rapid method for obtaining detailed refractive index profile measurements of graded-index fibres. A short length of fibre is illuminated with an incoherent source, and the index profile is determined by observation of the light-intensity variations across the fibre output face. To obtain an accurate index profile it is necessary to take into account the presence of tunnelling leaky-modes, which contribute additional power to the observed near-field intensity distribution [18, 19].

Light-intensity distributions were measured for short lengths ($\simeq 0.5$ to 1.0 m) of fibre taken from the middles of the five fibres described above. In addition as a check on reproducibility of the profiles, light-intensity distributions were also measured on short lengths of fibre taken approximately 200 m from the beginning and end of the five fibres. Fig. 1, solid curve, illustrates the near-field light-intensity distribution for a 1 m length of fibre taken from the middle of the phospho-silicate fibre VD/102.

Although an incoherent light source (a tungsten filament lamp) is used in the near-field scanning system, the convolution of the lamp spectral emission curve and detector response curve indicates that the measurements are effectively made at a wavelength region around $1 \mu m$.

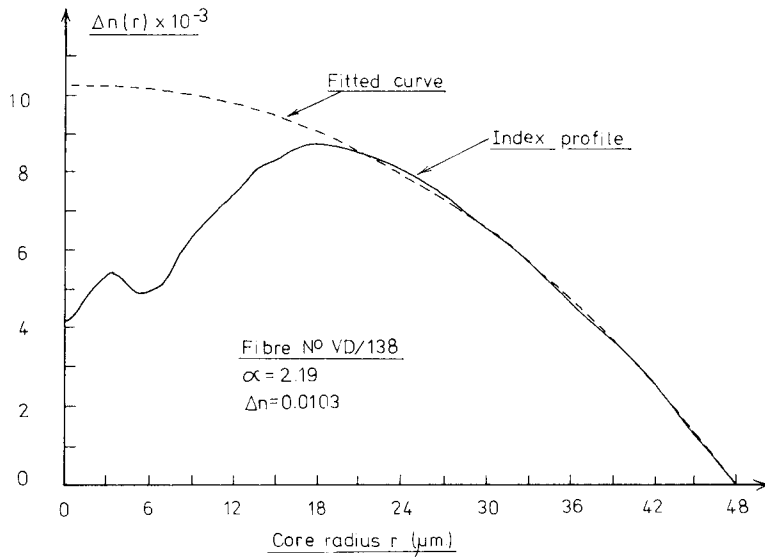The numerical aperture (NA) of each of the

Figure 2 Solid curve: absolute refractive index-difference profile for fibre VD/138. Dashed curve: function $\Delta n(r)$ fitted to refractive index-difference profile for fibre VD/138.

short lengths from the five different fibres was also determined with a He–Ne laser by fully exciting the fibre with a high NA launching lens, and measuring the output angle of the far-field radiation pattern.

3.2. Data processing

Finally the near-field intensity distributions were processed using computer programs developed on a Tektronix 4051 graphic systems computer.

Firstly each light-intensity distribution was corrected for the presence of leaky-modes to give a plot now directly related to the true refractive-index profile. The correction factor is a function of radial position in the core (r) and depends only on a single normalization parameter involving fibre length (z), core radius (a) and normalized frequency (v). The derivation and use of these correction factors are fully explained by [18] and [20]. Fig. 1, dashed curve, illustrates the plot relating directly to the refractive index, obtained after leaky-mode correction of the intensity profile. Using the core radius (a) and maximum refractive index difference Δn_m defined by the NA $[NA \simeq \sqrt{(2n_2 \Delta n_m)}]$ of the fibre, each corrected plot was scaled to give a plot of absolute refractive index difference (above or below the cladding index n_2) as a function of core radius: $\Delta n(r)$. Fig. 2, solid curve, illustrates $\Delta n(r)$ for the phosphosilicate fibre VD/138.

Secondly, using a curve fitting program, a mathematical expression of the form:

$$\Delta n(r) = \Delta n - Kr^\alpha \qquad (1)$$

was fitted to the data forming the plot $\Delta n(r)$. Although Equation 1 is not the best form of expression to fit to the data, because of the insensitivity of $\Delta n(r)$ to changes in α, it is useful for index-profile analysis as it explicitly contains the maximum index difference Δn and profile parameter α of the fibre. Fig. 2, dashed curve, illustrates the function $\Delta n(r)$ with $\alpha = 2.19$ and $n = 10.3 \times 10^{-3}$ fitted to the index-profile (solid curve) of fibre VD/138.

Thirdly, having reduced the index-profile data to a simple mathematical expression $\Delta n(r)$ and with a knowledge of the number of core layers deposited, it is now possible to define the boundaries of the layers in the core, in a method similar to that used by French *et al.* [21]. Assigning to each core layer its true concentration of dopant (P_2O_5, GeO_2 or B_2O_3) in the silica and by weighting the index difference of each layer between its boundary values, a graphical plot (or tabulation) of Δn (m) against true dopant concentration $(m \bmod \%)$ can be generated. Weighting is used to correct for dopant diffusion between adjacent layers, so that $\Delta n(m)$ is a monotonic function through the origin.
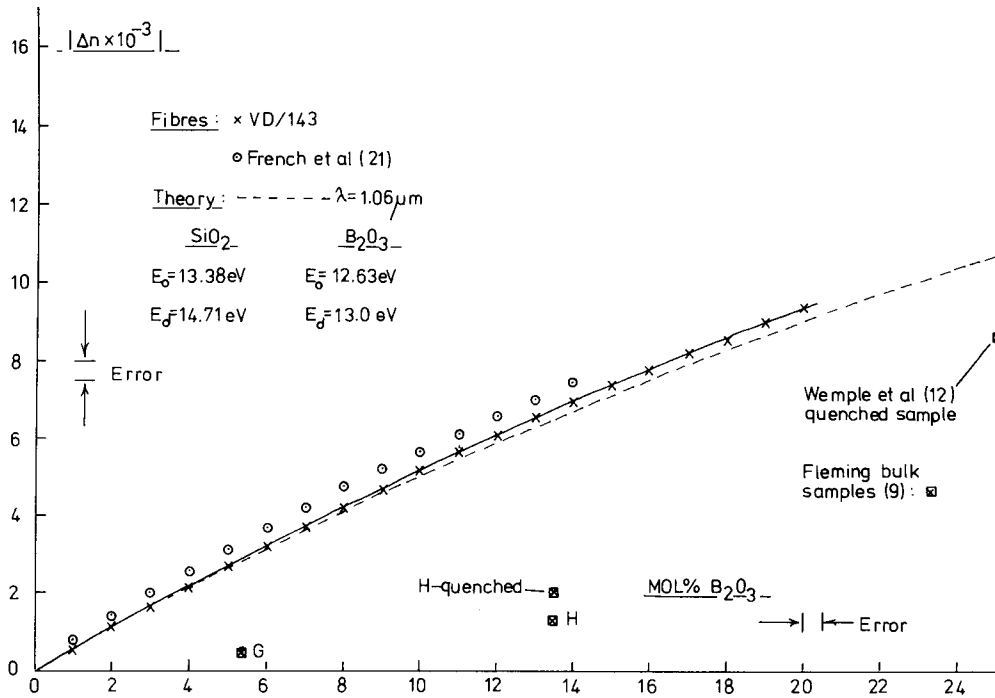
Figure 3 Solid curve: refractive index-difference as a function of mol % B_2O_3 for fibre VD/143. Dashed curve: Sellmeier model of $\Delta n\,(m)$ for $SiO_2 - B_2O_3$ glass at $\lambda = 1.06\,\mu m$.
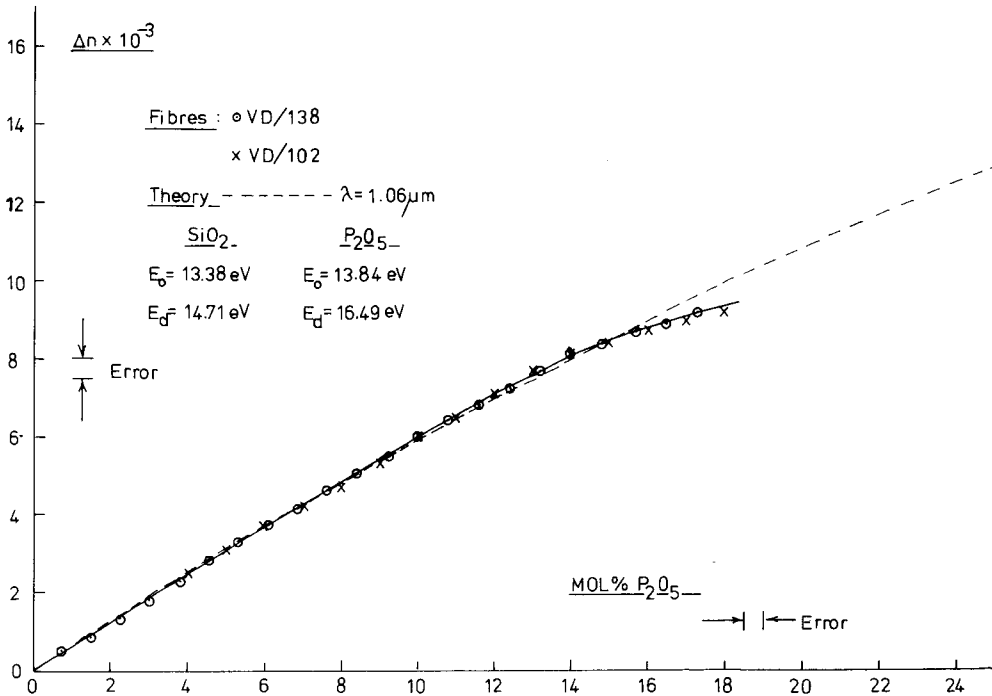

Figure 4 Solid curve: refractive index-difference as a function of mol % P_2O_5 for fibres VD/102 and VD/138. Dashed curve: Sellmeier model of $\Delta n\,(m)$ for $SiO_2 - P_2O_5$ glass at $\lambda = 1.06\,\mu m$.
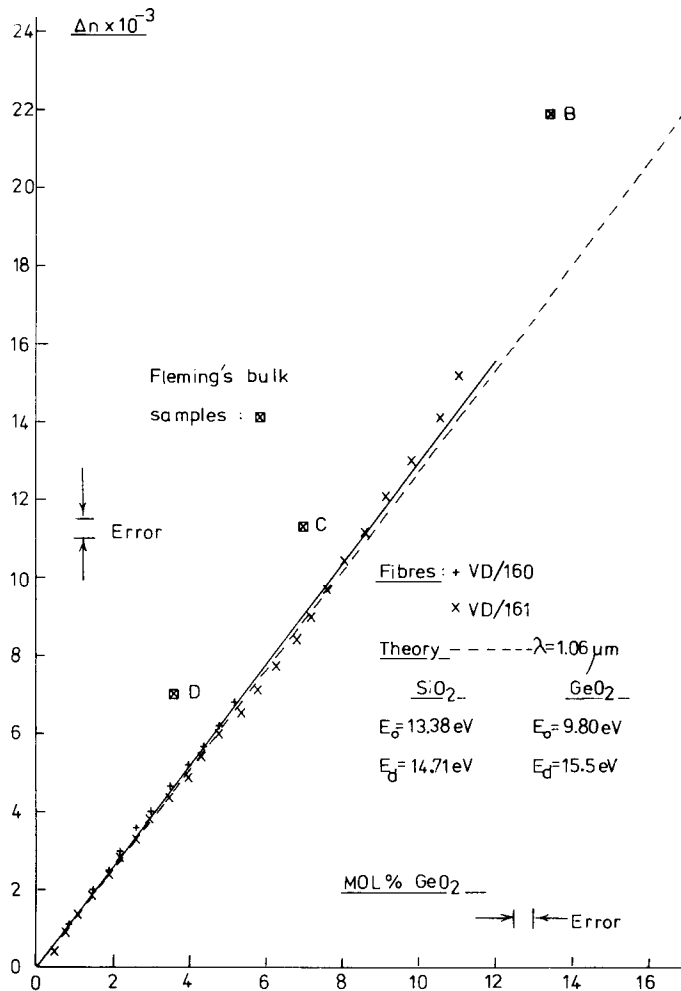
403

Figure 5 Solid curve: refractive index-difference as a function of mol % GeO_2 for fibres VD/160 and VD/161. Dashed curve: Sellmeier model of $\Delta n\,(m)$ for SiO_2-GeO_2 glass at $\lambda = 1.06\,\mu m$.

3.3. Results

Fig. 3 shows the variation of refractive index difference with composition $\Delta n\,(m)$ for the boro-silicate glass fibre VD/143, Fig. 4 $\Delta n\,(m)$ for the two phosphosilicate core fibres VD/102 and VD/138, and Fig. 5 $\Delta n\,(m)$ for the two germania-silicate core fibres VD/160 and VD/161. Included in Fig. 3 is $\Delta n\,(m)$ obtained by processing the refractive-index data (measured interferometrically) against composition of a graded-index $B_2O_3-SiO_2$ glass fibre presented by French *et al.* [21–23]. The agreement between these two sets of data for $\Delta n\,(m)$ for $B_2O_3-SiO_2$ glass is very good, and indicates that the near-field scanning technique gives results as accurate as the more laborious interferometric technique [23].

4. Sellmeier dispersion model

4.1. Formulation of the Sellmeier model

The refractive-index versus composition analysis used in the following is based on the theory developed by Wemple *et al.* [12] for bulk annealed samples of $SiO_2-B_2O_3$ glass. Use is made of the expression for refractive index in terms of a single Sellmeier oscillator of form:

$$n^2 - 1 = E_dE_o/(E_o^2 - E^2). \qquad (2)$$

E_o is the effective oscillator energy (near the fundamental UV absorption edge), E the photon energy, and E_d a dispersion energy (oscillator strength). The value of Equation 2 is based on the widely applicable empirical rules [24] obeyed by E_d and E_o. These allow an interpolation of the

404

TABLE I

Glass system	U	V
$x\mathrm{SiO_2}:1\mathrm{B_2O_3}$	$\dfrac{2x}{2x+3}$	$\dfrac{x}{x+2}$
$x\mathrm{SiO_2}:1\mathrm{P_2O_5}$	$\dfrac{x}{x+2}$	$\dfrac{x}{x+2}$
$x\mathrm{SiO_2}:1\mathrm{GeO_2}$	$\dfrac{x}{x+1}$	$\dfrac{x}{x+1}$

refractive index behaviour of the binary glass system, for example $x\mathrm{SiO_2}:1\mathrm{B_2O_3}$, based on properties of the end members-glassy $\mathrm{SiO_2}$ and $\mathrm{B_2O_3}$. For $E_o(x)$, the assumption is made that the oscillator energy is proportional to the fractional content of Si–O and B–O bonds U. Thus

$$E_o(x) = E_o(\mathrm{B_2O_3}) + U[E_o(\mathrm{SiO_2}) - E_o(\mathrm{B_2O_3})] \tag{3}$$

where

$$U = 2x/(2x+3) \text{ for } x\mathrm{SiO_2}:1\mathrm{B_2O_3}. \tag{4}$$

The dispersion energy E_d has been found to obey the empirical rule [24]

$$E_d = \beta N_c Z_a N_e \rho/\rho_c \tag{5}$$

where N_c is the cation coordination number, Z_a is the chemical valency of the anion (2 for oxides), N_e is the total number of valence electrons per anion (8 for the oxides considered), ρ/ρ_c is the ratio of the actual density of the glassy material to the density of the 'compacted' crystalline structure, and $\beta = 0.28\,\mathrm{eV}$ for 'ionic' bonded materials and $\beta = 0.38\,\mathrm{eV}$ for 'covalent' bonded materials [24]. Consequently the dispersion energy $E_d(x)$ depends on the fractional content of Si and B cations V, rather than the bond fraction U. Thus,

$$E_d(x) = E_d(\mathrm{B_2O_3}) + V[E_d(\mathrm{SiO_2}) - E_d(\mathrm{B_2O_3})] \tag{6}$$

where

$$V = x/(x+2) \text{ for } x\mathrm{SiO_2}:1\mathrm{B_2O_3}. \tag{7}$$

It is also assumed that density and index changes, resulting from quenching are only associated with the $\mathrm{B_2O_3}$ end member, since quenching of vitreous $\mathrm{SiO_2}$ produces relatively small changes in these two parameters (see [12]). Obviously for the other two glasses, U and V will take different forms (see Table I).

The essence of the analysis is to calculate E_d from Equation 5 for each of the end members, then using E_d and n_D (D-sodium line, $\lambda = 0.5893\,\mu m$) to calculate a corresponding E_o by solving Equation 2. E_o and E_d for the end members are then substituted into Equations 3 and 6 to yield $E_o(x)$ and $E_d(x)$, and inserting these latter two variables into Equation 2 finally results in $n(x)$. A modification is made in that molar %(m) is used as the composition variable in place of x where

$$m = 100/(1+x). \tag{8}$$

4.2. The dispersion energy and bonding considerations

Now we turn to the calculation of E_d for each of the four oxides. The basic structural building block of glassy $\mathrm{SiO_2}$, $\mathrm{P_2O_5}$ and $\mathrm{GeO_2}$ is the tetrahedron thus $N_c = 4$, whereas for glassy $\mathrm{B_2O_3}$ it is the planar triangle and thus $N_c = 3$ [25] (Table II).

Wemple and DiDomenico [24] state that all the six-coordinated oxides take the 'ionic' value of $\beta = 0.28\,\mathrm{eV}$, while the four-coordinated oxides seem to be either 'ionic' or 'covalent'. Consideration of the Allred–Rochow electronegativity differences [26] between O and Si, B, P and Ge is also useful in ascertaining the bond type of the four oxides. The electronegativity differences obtained (1.44 to 1.76) indicate that the bonds in the four oxides should have strong ionic characteristics [26]. Certainly for $\mathrm{SiO_2}$ it has been shown experimentally that β does indeed take the 'ionic' value of $\beta = 0.28\,\mathrm{eV}$ [12]. On the other hand Wemple *et al.* [12] have shown experimentally

TABLE II

Material	N_c	$\beta(\mathrm{eV})$	$\rho(\mathrm{g/cm^3})$	$\rho_c(\mathrm{g/cm^3})$	n_D	$E_d(\mathrm{eV})$	$E_o(\mathrm{eV})$
$\mathrm{SiO_2}$	4	0.28	2.212	2.65	1.4578	14.71	13.38
$\mathrm{B_2O_3}$	3	0.38	1.804	2.56	1.4355	13.00	12.63
$\mathrm{P_2O_5}$	4	0.28	2.176	2.365	1.490	16.49	13.84
$\mathrm{GeO_2}$	4	0.28	3.651	4.228	1.610	15.49	9.80

that B_2O_3 takes the 'covalent' value of $\beta = 0.38$ eV. GeO_2 can be six-coordinated [25] and phosphorus can be 5- or 6- coordinated [26], and because of the appreciable degree of ionic character of the bonds in GeO_2 and P_2O_5 [26], these two oxides were assigned the 'ionic' value of $\beta = 0.28$ eV. Table II summarizes the values of β assigned to the four oxides.

Finally it is necessary to assign appropriate values to the density ratio ρ/ρ_c in Equation 5 which is one of the key factors in predicting the refractive index behaviour of these quenched glasses.

4.3. Density and refractive index values for the model

The values of n_D and e for vitreous silica, and ρ_c for α-SiO_2 are well documented in the literature (see [12]). Density and refractive index data for the other three oxides in the glass form are less readily available, and some judgement has been exercised in selecting values appropriate to the highly quenched glass form.

For instance Vedam and Schneider [27] give $\rho = 1.833$ g/cm^3 and $n_D = 1.447$ for low-density (quenched) glassy B_2O_3, while Shelby [28] gives $\rho = 1.804$ g/cm^3 and $n_D = 1.458$. Scaling the value of $n_D = 1.447$ by the square root of the ratio of the densities ($n \propto \sqrt{\rho}$) gives that n_D should be $\simeq 1.436$ for ρ equal to 1.804 g/cm^3. Thus presumably Shelby's value of n_D is somewhat on the high side. The values $\rho = 1.804$ g/cm^3 and $n_D = 1.436$ were thus selected for computations on glassy B_2O_3 (see Table II) as being the most appropriate to the quenched glass form.

Few data are available for glassy P_2O_5, but Cormia et al. [29] give refractive index data for glassy and crystalline P_2O_5, and a relationship between temperature ($^\circ$ C) and the density of molten P_2O_5:

$$\rho = 2.372 - 3.38 \times 10^{-4}\ T(\text{g/cm}^3). \quad (9)$$

Assuming that quenched, glassy P_2O_5 would take the density of the melt at the melting temperature of 580° C [14] we estimate $\rho = 2.176$ g/cm^3 from Equation 9. Also from Cormia et al. [29] $n_D = 1.490$ was judged to be the most appropriate refractive index for quenched vitreous P_2O_5.

Finally for glassy GeO_2 the most appropriate density and refractive index that could be found

were $\rho = 3.651$ g/cm^3 and $n_D = 1.630$ from Morey [30] and Shelby [28]. Unfortunately no thermal history is given for the material used by Morey, and the specimens used by Shelby were well annealed.

Table II lists the values of n_D, ρ and ρ_c used to determine E_d and E_o for the end members, and their values for each vitreous material. Then using a computer program with the appropriate values of E_d and E_o (Table II), and U and V (Table I) for the end members, refractive index against composition $n(m)$ is obtained using Equations 3, 6 and 2. It is customary in fibre optics to use index differences rather than absolute indices, so Figs. 3–5 (dashed curves) give $\Delta n(m)$, calculated at $\lambda = 1.06\ \mu$m for the three binary glass systems under consideration. For pure SiO_2, $U = V = 1$ to give n(silica) = 1.4518 (at 1.06 μm), so that $\Delta n(m)$ equals $n(m) - 1.4518$ for each binary glass.

5. Discussion
5.1. SiO_2–B_2O_3 and SiO_2–P_2O_5 glasses

Quenched SiO_2–B_2O_3 glass has refractive indices less than those of vitreous silica and hence its common use as a cladding glass for optical fibres. Fig. 3 shows that good agreement is obtained between the measured values of $\Delta n(m)$ (solid curve) and the values calculated from the Sellmeier model (dashed curve), over the composition range considered – up to 20 mol % B_2O_3. At this concentration the measured value of $|\Delta n(m)/n(SiO_2)|$ is 0.65 %, which agrees with the figure of 0.6% measured by Wemple et al. [12] for a quenched 25 mol % B_2O_3 sample, see Fig. 3. More generally the shape of our $\Delta n(m)$ curve, for both measured and theoretical values, is consistent with that obtained by Wemple et al. [12] for low density SiO_2–B_2O_3 glass. The severe quenching inherent in the fibre drawing process here greatly increases the value of Δn obtained from a given composition by considerably lowering $n(m)$ with respect to $n(SiO_2)$. As an illustration of this, Fig. 3 also contains data points obtained from measurements made by Fleming [9] on two bulk samples of SiO_2–B_2O_3 glass – points G and H. Thus quenching in this system is very advantageous when using these glasses as claddings for optical fibres. Finally measurements on other fibres fabricated in these laboratories indicate that even greater values of $|\Delta n(m)|$ can be obtained for B_2O_3 levels above
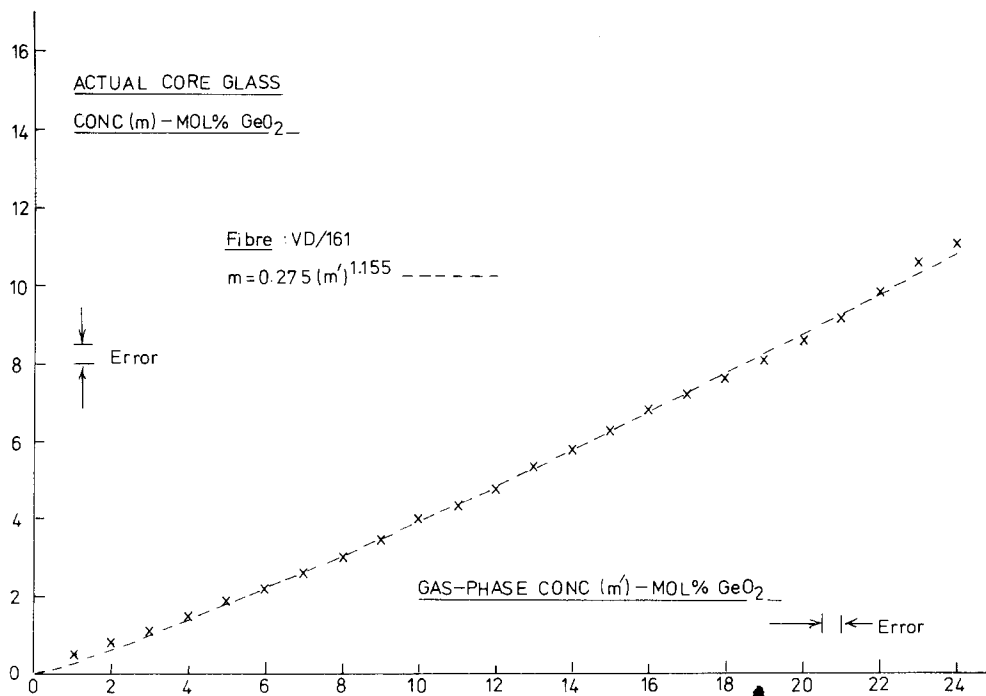
Figure 6 Actual GeO_2 concentration in fibre VD/161 (m) as a function of set gas-phase concentration (m').

20 mol %, before the limit imposed by expansion coefficient considerations is reached.

Also agreement between experimental values and theoretical calculations for quenched $SiO_2-P_2O_5$ glass is extremely good for compositions up to 20 mol % P_2O_5, Fig. 4. Results from other fibres fabricated in these laboratories indicate that 25 mol % is the maximum amount of P_2O_5 that can be incorporated in this glass system, because of expansion coefficient mis-match. At this composition $\Delta n(m)/n(SiO_2)$ is equal to 0.9%. Quenching in this glass system has the effect of decreasing the value of $\Delta n(m)$ obtained from a given composition by lowering $n(m)$ with respect to $n(SiO_2)$, which is to some extent a disadvantage when using $SiO_2-P_2O_5$ glass for a fibre core. Fig. 4 also indicates some departure of the glass composition away from the vapour-phase composition at high P_2O_5 concentrations (> 15 mol % P_2O_5).

5.2. SiO₂–GeO₂ glasses

Initially little agreement was found between the measured refractive index differences as a function of gas-phase composition, and calculations made from the Sellmeier model for quenched SiO_2-GeO_2 glass. However, fairly good agreement was

obtained between the Sellmeier model and refractive index measurements made by Fleming [9], on bulk samples of SiO_2-GeO_2 glass prepared by r.f. plasma fusion (see Fig. 5). This lack of consistency between fibre core glass measurements and bulk glass measurements suggested that the SiO_2-GeO_2 core glass composition was greatly different from that set by the vapour streams in this particular CVD process.

Measurements made with a JEOL microprobe analyser (JXA–50A) by counting the K_α, X-ray emission from the Ge in a fibre core against that from a pure Ge reference sample, supported the above supposition. For instance fibre VD/160 fabricated to have a maximum of 15 mol % GeO_2 in the gas-phase was found actually to have a maximum core doping of only 5 mol % GeO_2. Fibre VD/161 with a gas-phase maximum of 24 mol % GeO_2 was found to have a maximum GeO_2 concentration in the core of ~ 11 mol %. Consequently the microprobe analyser was used to obtain Ge concentration profiles of the fibre cores, and from these the true doping level of GeO_2 for each deposited core layer was determined. Fig. 6 illustrates how the actual concentration of GeO_2 in the core glass (m) varies as a

407

function of the set gas-phase concentration (m') for VD/161. Here for $m > 2$ mol % GeO_2 the curve is described by the relation

$$m = 0.275(m')^{1.155}. \qquad (10)$$

The exact relationship between m and m' varies from fibre to fibre and is obviously dependent on the deposition conditions, particularly the deposition temperature. It has been found experimentally that the higher the deposition temperature the lower is the amount of GeO_2 incorporated in the core glass from the gas-phase. For the deposition temperatures we use for GeO_2 ($\sim 1500°$ C) a good approximation is that $m \simeq 0.3\,m'$. Similar observations on SiO_2–GeO_2 glass have been made by Isobe [31].

Fig. 5, solid curve, shows the measured variation of refractive index with actual GeO_2 concentration $\Delta n(m)$ for the two fibres VD/160 and VD/161. Agreement between the experimental measurements and the theoretical calculations for SiO_2–GeO_2 glass from the Sellmeier model (dashed curve) is again extremely good. Again the effect of quenching on the SiO_2–GeO_2 glass system has been to lower the values of $\Delta n(m)$ obtained, by about 2×10^{-3} below the data points obtained from Fleming's measurements on bulk samples B, C and D [9].

At the maximum GeO_2 concentration obtained here, i.e. 11 mol % GeO_2, $\Delta n(m)/n(SiO_2)$ is about 1 %, thus the refractive index differences for the SiO_2–GeO_2 glass system are about three times that obtained for the same doping levels in the SiO_2–P_2O_5 glass system. However, the reduction in GeO_2 concentration by about one third between the gas-phase and the glass in CVD, means that for equivalent gas-phase compositions the refractive index differences obtained are roughly the same for either glass system, i.e. 25 mol % P_2O_5 yields $\Delta n = 13 \times 10^{-3}$ while 11 mol % $GeO_2 \equiv 24$ mol % GeO_2 in the gas-phase yields $\Delta n = 14 \times 10^{-3}$.

6. Conclusion

Analysis of the refractive index behaviour of the binary glasses: SiO_2–B_2O_3, SiO_2–P_2O_5 and SiO_2–GeO_2 in the quenched condition present in fibres, has shown that the observed dependence on composition can be explained in terms of properties of the end-member glasses. Provided that in

the Sellmeier model the effects of quenching on the properties of the end-members B_2O_3, P_2O_5 and GeO_2 are considered, and that the true fibre dopant concentrations, particularly for GeO_2, are used in the model. It should be mentioned that an alternative analysis based on the molar-refractivity concept [32] has not been attempted, since preliminary calculations based on this model gave only rather qualitative results for these three glass systems.

The Sellmeier model has also been used to determine doping programmes to fabricate fibres with profiles having given alpha values [33]. An extension to the model has been made with the addition of a second infra-red Sellmeier oscillator term having a second pair of composition dependent energies E'_o and E'_d. This refinement has enabled calculations to be made of pulse broadening, profile dispersion and optimum alpha value [7] as a function of wavelength for these three glass systems [33].

References

1. D. N. PAYNE and W. A. GAMBLING, *Elect. Lett.* **10** (1974) 289–90.
2. P. W. BLACK, J. IRVEN, K. BYRON, I. S. FEW and R. WORTHINGTON, *ibid.*, **10** (1974) 239–40.
3. W. G. FRENCH, J. B. MACCHESNEY, P. B. O'CONNOR and G. W. TESKER, *Bell Syst. Tech. J.* **53** (1974) 951–4.
4. W. G. FRENCH, D. A. PEARSON, G. W. TASKER and J. B. MACCHESNEY, *Appl. Phys. Lett.* **23** (1973) 338–9.
5. J. B. MACCHESNEY, R. E. JAEGER, D. A. PINNOW, F. W. OSTERMAYER, T. C. RICH and L. G. VAN UITERT, *ibid.*, **23** (1973) 340–1.
6. D. GLOGE and E. MARCATILI, *Bell Syst. Tech. J.* **52** (1973) 1563–78.
7. R. OLSHANSKY and D. B. KECK, *Appl. Opt.* **15** (1976) 483–91.
8. J. A. ARNAUD and J. W. FLEMING, *Elect. Lett.* **12** (1976) 167–9.

9. J. W. FLEMING, Fall Meeting of the American Ceramic Society, Pocono Manor (Pennsylvania) (1975).

10. D. GLOGE, I. P. KAMINOW and H. M. PRESBY, *Elect. Lett.* **11** (1975) 469–71.

11. L. G. COHEN, *Appl. Opt.* **15** (1976) 1808–14.

12. S. H. WEMPLE, D. A. PINNOW, T. C. RICH, R. E. JAEGER and L. G. VAN UITERT, *J. Appl. Phys.* **44** (1973) 5432–37.

13. N. MOCHIDA and K. TAKAHASHI, Proc. Tenth Int. Congress on Glass 13 (Kyoto, Japan, 1974) 29–35.

14. W. H. OTTO, *J. Am. Ceram. Soc.* **44** (1961) 68–72.

15. W. A. WEYL and C. E. MARBOE, *The Constitution of Glasses.* Vol. 2, Part 1, Chapter 21, pp. 863–71 (Wiley, New York, 1964).

16. W. A. GAMBLING, D. N. PAYNE, C. R. HAMMOND and S. R. NORMAN, *Proc. IEE* **123** (1976) 570–6.

17. D. N. PAYNE and W. A. GAMBLING, *Bull. Am. Ceram. Soc.* **55** (1976) 195–7.

18. F. M. E. SLADEN, D. N. PAYNE and M. J. ADAMS, *Appl. Phys. Lett.* **28** (1976) 255–8.

19. M. J. ADAMS, D. N. PAYNE and F. M. E. SLADEN, *Elect. Lett.* **11** (1975) 389–91.

20. *Idem. Opt. Commun.* **17** (1976) 204–9.

21. W. G. FRENCH, G. W. TASKER and J. R. SIMPSON, *Appl. Opt.* **15** (1976) 1803–7.

22. L. G. COHEN, G. W. TASKER, W. G. FRENCH and J. R. SIMPSON, *Appl. Phys. Lett.* **28** (1976) 391–3.

23. P. D. LAZAY, J. R. SIMPSON, W. G. FRENCH and B. C. WONSIEWICZ, First European Conference on Optical Fibre Communications, IEE, London (1975).

24. S. H. WEMPLE and M. DIDOMENICO, *Phys. Rev.* **B3** (1971) 1338–51.

25. R. H. DOREMUS, *Glass Science,* Chapter 3, pp. 23–27 (Wiley, New York, 1973).

26. L. D. PYE, H. J. STEVENS and W. C. LACOURSE, *Introduction to Glass Science* Chapter 2, pp. 31–60 (Plenum Press, New York, 1972).

27. K. VEDAM and W. C. SCHNEIDER, *J. Appl. Phys.* **43** (1972) 3623–7.

28. J. E. SHELBY, *ibid.,* **45** (1974) 5272–7.

29. R. L. CORMIA, J. D. MACKENZIE and D. TURNBULL, *ibid.,* **34** (1963) 2245–8.

30. G. W. MOREY, *Properties of Glass* Chapters 11 and 16 (Reinhold, New York, 1954).

31. T. ISOBE, Furukawa Electrical Co. Ltd., Report (1976).

32. M. BORN and E. WOLF, *Principles of Optics* Chapters 2 and 3 pp. 87–8 (Pergamon Press, Oxford, 1970).

33. C. R. HAMMOND, (to be published).